Full waveform inversion of transient electromagnetic data in the time domain

Junjie Xue, *Jiulong Cheng, Leiv-J. Gelius, Xing Wu, Yang Zhao

Abstract—Quasi-seismic imaging is a popular form of electromagnetic imaging technology. In most cases, it is considered that it will yield more obvious layered characteristics if the electromagnetic response is transformed into the virtual wave domain. However, the time profile of virtual wave cannot effectively show the underground electromagnetic structure before migration. In this paper, we make an improvement to process the virtual wave, by applying the full waveform inversion method, with the steps detailed as follows: (1) we use the truncated singular value decomposition method to transform the transient electromagnetic response to the virtual wave field. (2) Using the FDTD method, we calculate the virtual wave field according to the resistivity model, then use the shearlet transform to remove the direct wave. (3) We use a least square equation between the virtual wave and transformed virtual wave to express the problem of full waveform inversion. Next, we apply one of steepest descent methods—the Marquardt approach—to obtain the optimal underground conductivity information. Finally, we use the synthetic and field data to show the accuracy and rationality of the method proposed in this paper.

Index Terms—quasi-seismic, virtual wave field, full waveform inversion, transient electromagnetic field

I. INTRODUCTION

THE transient electromagnetic method (TEM) has been widely applied in resource, environment and engineering detection [1][2][3]. It involves setting the loop or finite long wire source in the ground to excite an initial electromagnetic field. Then, during the interval of primary pulse, the coil or ground electrode is used to collect field data and reveal the underground resistance structure distribution [4].

Junjie Xue is employed at the State Key Laboratory of Coal Resources and Safe Mining, China University of Mining & Technology (Beijing), Beijing 100083, China. (e-mail: junjie_58@126.com)

Jiulong Cheng is employed at the State Key Laboratory of Coal Resources and Safe Mining, China University of Mining & Technology (Beijing), Beijing 100083, China. (e-mail: jlcheng@cumtb.edu.cn)

Leiv-J. Gelius is employed at the Department of Geosciences, University of Oslo, 0315 Oslo, Norway. (e-mail: l.j.gelius@geo.uio.no)

Xin Wu is employed at the Key Laboratory of Mineral Resources, Institute of Geology and Geophysics, Chinese Academy of Sciences, Beijing 100029, China, and also at the College of Earth and Planetary Sciences, University of Chinese Academy of Sciences. Beijing 100049, China. (e-mail: wu_xin@163.com)

Yang Zhao is employed at the Key Laboratory of Mineral Resources, Institute of Geology and Geophysics, Chinese Academy of Sciences, Beijing 100029, China, and also at the College of Earth and Planetary Sciences, University of Chinese Academy of Sciences. Beijing 100049, China. (e-mail: zhaoyang0320@mail.iggcas.ac.cn)

In practical work involving the observed induced secondary field data, it always uses the resistivity fitting to perform the inversion, then uses the approximate formulas for the apparent resistivity imaging. However, this method may lead to interpretation errors, which occur due to the volume effect and inaccuracy of the approximate formula [5].

Learning from the mature technology of seismic exploration is a development direction for TEM [6]. The seismic method features high resolution, and can be used to accurately image the subsurface structures by employing migration techniques [7][8][9]. At the same time, time-domain EM techniques can be used to determine the apparent resistivity of the underground, yet with poor depth resolution due to the diffusive character of the EM wave fields [10][11]. There is an integral relationship between the diffusive equation and wave equation [12][13], and previous research has mostly focused on obtaining a high resolution inverse result of virtual wave data, such as piecewise integration [14] and optimization, synthetic-aperture type of processing [15] and Kirchhoff [16] migration. Moreover, this technic can be further applied to the underground electromagnetic exploration [17][18]. The full waveform inversion (FWI) approach is an efficient tool for migration imaging, and can be used to obtain a high resolution of underground structure by continuing to fit the calculated values and field data. At present, FWI has been applied to the inversion of ground radar wave [19][20], transmitted waves [21] SH waves, Love waves [22], and so on. However, an FWI method for deep electromagnetic migration imaging has yet to appear.

In the present paper, we adapt the virtual wave field idea to obtain better-resolved electric earth models. Next, we propose applying the concept of full waveform inversion (FWI), a technique well known from the seismic community and used to estimate the seismic parameters of the underground, based on a least-squares object function [23]. By analogy with seismic FWI, we propose the use of EM based FWI employing virtual wave fields as the input data to alternatively recover the electric parameters. We employ both the simulation data and field data to demonstrate the potential of the proposed methodology.

II. RELATIONSHIP BETWEEN THE UNDERGROUND RESISTIVITY AND TRANSIENT ELECTROMAGNETIC VIRTUAL WAVE FIELD

A. Virtual wave field equation in the time-domain

Taking the Maxwell equations as a starting point, it can be readily demonstrated that the electromagnetic field satisfies the diffusion equation [12]:

$$\nabla^2 E(t) - \mu\sigma \frac{\partial E(t)}{\partial t} = S_E(t) \tag{1}$$

where S_E represents the source function, μ is the permeability of vacuum, σ is the electrical conductivity, E is the electric field intensity, and t represents time.

In his work, Lee [12] introduced the concept of a virtual wave, which is a solution to the acoustic wave equation used in seismic propagation. More importantly, he demonstrated that the following relationship exists between the electromagnetic field and the virtual wave:

$$E(t) = \frac{1}{2\sqrt{\pi t^3}} \int_0^\infty q e^{\frac{-q^2}{4t}} U(q)dq \tag{2}$$

where U is the virtual wave, and q is the virtual time. Note that the unit of virtual time is $\sqrt{s}$. Combining Equations (1) and (2) yields the virtual wave field equation in time:

$$\nabla^2 U(q) - \mu\sigma \frac{\partial^2 U(q)}{\partial q^2} = F(q) \tag{3}$$

with F representing the transformed source function. We follow the original work of [12] and represent F by a Gaussian excitation function:

$$F(q) = e^{-(q-q_0)^2/2\alpha^2} \tag{4}$$

The smaller the value of the parameter α in Equation (4) is, the sharper peak of the source function will be. The excessively small α leads to numerical instabilities in the finite-difference computations. From our extensive testing, we observed that the following parametric choice of q_0=0.03 and α =0.005 worked quite well [12].

B. Finite-difference solution

In this paper, we solve Equation (3) by employing finite-difference modeling, and use a central-difference operator for the second derivative, as follows:

$$\frac{\partial^2 f}{\partial x^2} \cong \frac{f(x+\Delta x) + f(x-\Delta x) - 2f(x)}{\Delta x^2} \tag{5}$$

Introducing this operator to Equation (3) yields the corresponding discrete version of the wave equation:

$$U_{i,j}^{k+1} = \frac{\left(\frac{U_{i+1,j}^k + U_{i-1,j}^k - 2U_{i,j}^k}{\Delta x^2} + \frac{U_{i,j+1}^k + U_{i,j-1}^k - 2U_{i,j}^k}{\Delta z^2} - F(q) \right)}{\mu\sigma} \Delta q^2 + 2U_{i,j}^k - U_{i,j}^{k-1} \tag{6}$$

where index i represents the (discretized) lateral spatial coordinate x, and index j is the corresponding depth coordinate z. Finally, index k represents the virtual time q. The increment in q is strictly dictated by the Courant-Friedrichs-Lewy (CFL) stability condition for hyperbolic equations [1]. In the case of a 2D finite-difference scheme, the q increment is given explicitly, as follows [12]:

$$\Delta q_{max} = 0.44\alpha \frac{v_{min}}{v_{max}} \tag{7}$$

where v_{min} and v_{max} represent respectively the minimum and maximum velocity, and the velocity is computed using the expression $1 / \sqrt{\mu\sigma}$.

III. SIMULATION PRINCIPLE OF VIRTUAL WAVE FIELD

In physical cases, the virtual wave field propagates without any borders. This is not the case in finite-difference modeling, where artificial boundaries must be introduced to limit the computational burden. Therefore, we must select the most suitable boundary conditions.

A. Boundary condition at ground-air interface

The upper boundary is represented by the ground-air interface where the conductivity of the air layer is very low, and set as 0.00001 s/m. Based on theoretical considerations, it follows that the boundary condition associated with this interface can be written as follows [25]:

$$\frac{\partial}{\partial z} U(x, z=0, q) = \frac{1}{\pi} \int_{-\infty}^{+\infty} dx' \frac{\partial_x U(x', z=0, q)}{x - x'} \tag{8}$$

B. Absorbing boundary conditions

Along the remaining boundaries, absorbing boundary conditions are employed to avoid artificially reflected waves. When the waves propagate inside the absorbing layers, then the total virtual wave field will be attenuated along both the horizontal direction x and vertical direction z, by introducing artificial diffusion terms:

$$\frac{\partial^2 U_x}{\partial t^2} + 2d_x \frac{\partial U_x}{\partial t} + d_x^2 U_x = v^2 \frac{\partial^2 U_x}{\partial x^2} \tag{9}$$

$$\frac{\partial^2 U_z}{\partial t^2} + 2d_z \frac{\partial U_z}{\partial t} + d_z^2 U_z = v^2 \frac{\partial^2 U_z}{\partial z^2} \tag{10}$$

with v representing the velocity of the virtual wave field. In Equations (10) and (11), d_x and d_z are the attenuation factors [7].

C. Direct waves

The virtual wave field computed by finite-difference time-domain modeling will be dominated by direct waves. Therefore, such contributions must be removed from the data before they can be used in FWI. In most cases, a linear time-gate always is used to remove the direct wave. However, the reflecting waves from the underground targets and the direct wave sometimes overlap when the targets are buried shallowly. In this section, we use the shearlet transform (ShT) to remove the direct wave, of which we give a simple introduction here.

ShT is a type of new multiple scale and directions geometric analysis technique. A shearlet system includes a scaling matrix, either A_{2^j} or $\tilde{A}_{2^j}$, and a shearing matrix S_k:

$$A_{2^j} = \begin{pmatrix} 2^j & 0 \\ 0 & 2^{j/2} \end{pmatrix} \quad \tilde{A}_{2^j} = \begin{pmatrix} 2^{j/2} & 0 \\ 0 & 2^j \end{pmatrix} \quad S_k = \begin{pmatrix} 1 & k \\ 0 & 1 \end{pmatrix} \tag{11}$$

where j is the scale parameter, and k is the shear parameter.

The definition of the shearlet system can be expressed by a scaling function $\phi \in L^2(R)$ and shearlets: ψ, $\tilde{\psi} \in L^2(R)$ as follows [26]:

$$SH(\phi,\psi,\tilde{\psi};c) = \Phi(\phi;c) \cup \Psi(\psi;c) \cup \tilde{\Psi}(\tilde{\psi};c) \qquad (12)$$

where $c = (c_1, c_2) \in (R^+)^2$ denotes the sampling parameter.

$$\Phi(\phi;c) = \left\{ \phi_m = \phi(\cdot - c_1 m) : m \in \mathbb{Z}^2 \right\}$$

$$\Psi(\psi;c) = \left\{ \psi_{j,k,m} = 2^{\frac{3j}{4}} \psi(S_k A_{2j} \cdot - M_c m) : j \geq 0, |k| \leq \left[2^{j/2}\right], m \in \mathbb{Z}^2 \right\}$$

$$\tilde{\Psi}(\psi;c) = \left\{ \tilde{\psi}_{j,k,m} = 2^{\frac{3j}{4}} \tilde{\psi}(S_k^T \tilde{A}_{2j} \cdot - \tilde{M}_c m) : j \geq 0, |k| \leq \left[2^{j/2}\right], m \in \mathbb{Z}^2 \right\}$$

$$M_c = \begin{pmatrix} c_1 & 0 \\ 0 & c_2 \end{pmatrix} \quad \tilde{M}_c = \begin{pmatrix} c_2 & 0 \\ 0 & c_1 \end{pmatrix}$$

Setting

$$\Lambda = \left\{ (j,k,m) : j \geq 0, |k| \leq [2^{j/2}], m \in Z^2 \right\} \qquad (13)$$

Therefore, the discrete shearlet transform can be defined by $SH_{\phi,\psi,\tilde{\psi}} f : Z^2 \times \Lambda^3 \to C^3$ of some function $f \in L^2(R^2)$

$$SH_{\phi,\psi,\tilde{\psi}} f(m,(j,k,m),(\tilde{j},\tilde{k},\tilde{m})) = \left(\langle f, \varphi_m \rangle, \langle f, \psi_{j,k,m} \rangle, \langle f, \tilde{\psi}_{\tilde{j},\tilde{k},\tilde{m}} \rangle \right) \qquad (14)$$

where L represents a set of integers.

Next, the approach of direct wave remove is introduced.

The direct wave r can be expressed as follows [26]:

$$r(x,t) = r_1(t) r_2(x) \qquad (15)$$

where r_1 and r_2 are the time and space components, respectively.

To remove the direct wave, first the virtual wave is transformed to the frequency domain by Equation (14). Then, a time window is used to make the ShT coefficients related to the direct wave become zero, as follows:

$$SH_{\phi,\psi,\tilde{\psi}} r_1 = 0 \qquad (16)$$

Next, the virtual wave data of free direct wave can be obtained by the inverse ShT method.

To justify this choice, we assume a simple earth model with one interface. Fig. 1(a) shows the geological model for the test, the red circle represents the source, and the black triangles represent receivers. Fig. 1(b) shows the complete virtual wave response in case the depth down to the reflecting layer is 20 m. The application of ShT transform gives the result shown in Fig. 1(c), where we observe that the reflection is completely recovered.
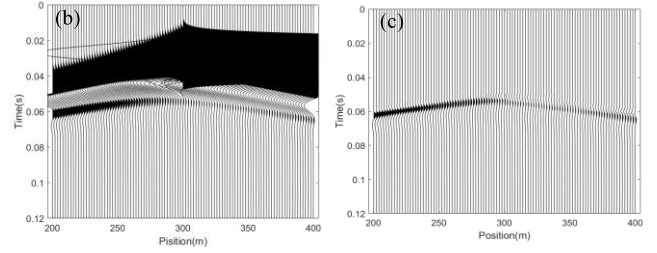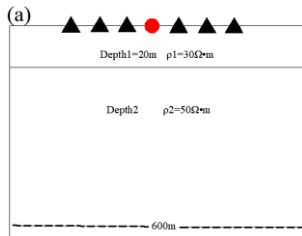

Fig. 1. Virtual wave field time-response: (a) model diagram for 20 m of first layer; (b) total response with interface at the 20 m depth; (c) after removal of direct wave.

D. Comparison the virtual wave and the seismic wave

To illustrate the effectiveness of the virtual wave, we set an abnormal body model, as shown in Figs. 2(a) and (b). Based on our previous experience, we use the velocities 2,000 m/s and 3,000 m/s to respectively correspond to the resistivity of 30 Ω•m and 50 Ω•m. Then we simulate the virtual wave propagation Equation (6) and the elastic wave propagation in seismology [27].

A clear vertical interface is shown in Figs. 2(c)–(d). Although there are some interference waves present in Fig. 2(a), it still has a sufficiently good ability to show the vertical interface of the abnormal body position.
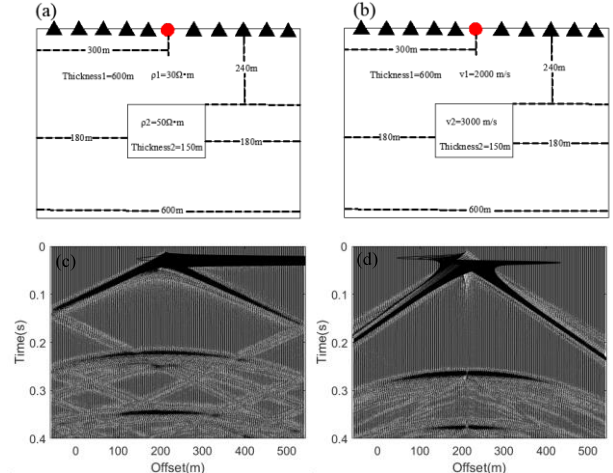

Fig. 2. Comparison the virtual wave and the seismic wave response: (a) model diagram with resistivity; (b) model diagram with velocity; (c) time profile of the virtual wave; (d) time profile of the seismic wave.

IV. FULL WAVEFORM INVERSION FOR UNDERGROUND RESISTIVITY

A. Inverse wave transform

This is an ill-posed problem for the inverse problem of Equation (2). To obtain a high-resolution result, some regularization methods can be used to solve this problem, such as damped least squares, truncated singular value decomposition (TSVD) [29], etc.

This paper uses the TSVD method to solve the inverse problem of Equation (2), and then we provide a simple introduction of TSVD.

The discrete form of Equation (2) can be expressed as follows:

$$E = AU \qquad (17)$$

where E, A and U respectively represent the discrete form of electromagnetic data, coefficient matrix and the virtual wave data.

Using the singular value decomposition to express the coefficient matrix:

$$A = \sum_{i=1}^{n} p_i \sigma_i v_i{}'$$ (18)

where p_i and v_i respectively represent the left and right singular vectors.

Adding TSVD to Equation (17), the virtual wave U can be expressed as follows:

$$U \approx \sum_{i=1}^{k} \frac{(E, v_i) p_i{}'}{\sigma_i}$$ (19)

where k is the constant of truncated position.

B. Full waveform inversion (FWI)

According to the least squares method, the object function of FWI is as follows:

$$\Phi = \|d - F(m)\|_2 + \lambda \|m\|_2$$ (20)

where d is the observed data, F is the virtual wave forward operator matrix, m is the parameter for inversion, and λ is a regularization factor.

With the time-domain virtual wave field as the input, a full waveform inversion is then carried out based on an iterative Marquardt approach [30]:

$$\Delta m = (\lambda I + J^T J)^{-1} (J^T \Delta y)$$ (21)

where Δm is the update in resistivity, I is the unit matrix, and Δy represents data fitting error. Moreover, J is the Jacobian, and represents the quantity $\partial U / \partial \rho$, where ρ is the resistivity.

Taking the derivative with respect to resistivity on both sides of Equation (3) yields the following partial differential equation for the Jacobian:

$$\nabla^2 J(q) - \mu\sigma \frac{\partial^2 J(q)}{\partial q^2} + \mu\sigma^2 \frac{\partial^2 U(q)}{\partial q^2} = 0$$ (22)

Then, its corresponding discrete form is given as follows:

$$J_{i,j}^{k+1} = \frac{\left(\frac{J_{i+1,j}^k + J_{i-1,j}^k - 2J_{i,j}^k}{\Delta x^2} + \frac{J_{i,j+1}^k + J_{i,j-1}^k - 2J_{i,j}^k}{\Delta z^2} + \mu\sigma^2 \frac{U_{i,j}^{k+1} + U_{i,j}^{k-1} - 2U_{i,j}^k}{\Delta z^2} \right)}{\mu\sigma}$$
$$\cdot \Delta q^2 + 2J_{i,j}^k - J_{i,j}^{k-1}$$ (23)

where the same indexes have been used as in Equation (6). Therefore, Equation (20) is employed to update the Jacobian after each iteration.

We then utilize the root mean square (RMS) to update the regularization factor λ:

$$Rms = \frac{1}{N_T N_D} \sqrt{\sum_{1}^{N_D} (d - F(m))^2}$$ (24)

$$\lambda = \begin{cases} \lambda * 2, & if \quad Rms \uparrow \\ \lambda / 2, & if \quad Rms \downarrow \end{cases}$$ (25)

Table 1 is the inversion flow of the proposed method in this paper.

TABLE I
WORKFLOW

Step 1:	Input the initial model λ and observed TEM data.
Step 2:	Use TSVD method to invert the observed TEM data to the virtual wave data.
Step 3:	Calculate the Jacobin matrix J, initial model response F and fitting error.
Step 4:	Update the model parameters according to Equation (20).
Step 5:	Update regularization factor λ according to Equations (23) and (24), then return step 3.

V. SIMULATION DEMONSTRATIONS

In actual field experiments of TEM data, large-loop transmitter systems are employed. However, the inversion approach advocated in this paper assumes point source data. Therefore, we must first justify the use of our approach in the case of field measurements. Next, we introduce a normal regularization method to obtain the virtual wave data from Equation (2). Finally, we investigate two controlled earth models, and demonstrate the potential performance of our proposed method.

A. Comparison of forward and inversed virtual wave field

In this section, we illustrate the rationality of using the virtual wave field with a point source to explain the inversed virtual wave field with loop source. A layered model is set up, as shown in Figs. 3(a)–(d), where the black triangles represent receivers, and the red circles represent transmitters in different positions.

First, we use 1D numerical simulation to obtain the TEM response of the model (Fig. 3(a)). Then the virtual wave data of loop antenna and point source can be respectively obtained by Equations (17) and (6).

To avoid the difference of magnitude and time, normalization is used as follows:

$$U_i = \frac{U_i}{\max(U)}, \quad i = 1, 2, \ldots n$$ (26)

$$T_i = T_i + \alpha, \quad i = 1, 2, \ldots n$$ (27)

where T represents the time of virtual wave data with loop antenna.

After removing the direct wave by ShT transform, the results of a comparison between the forward and inversed virtual wave response are shown in Figs. 3(c) – (f). We then take the response from the eighth receiver with different source positions. From Figs. 3(c) – (e), it can be seen that not all of them fit well in either the late or early time period. Fig. 3(f) shows that with a combination of three sources, superior fitting results are obtained throughout the time period.
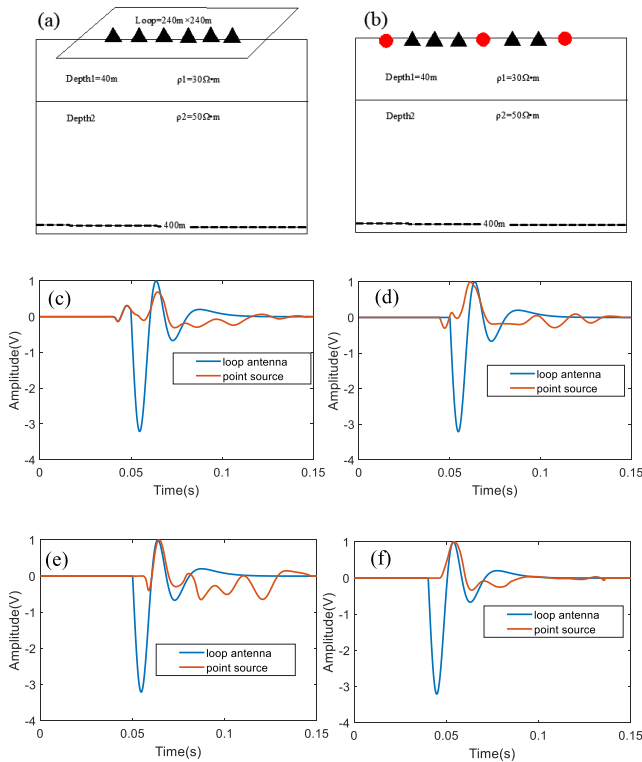
Fig. 3. Calculated TEM responses of point source and loop source: (a) layout of TEM; (b) layout of virtual seismic with source at 120 m, 200 m and 280 m; (c)–(e) comparison of the eighth receiver of virtual and inversed virtual wave; (f) multisource comparison.

B. Synthetic test

To illustrate the flow of the algorithm proposed in this paper, it is greatly preferable to begin with the transient electromagnetic response with resistivity model. Model 1 consists of three layers with the highest resistivity in the middle layer. The model parameters are illustrated in Figs. 4(a) and (b), where the black triangles represent the receivers, and the red circles respectively represent the point sources in the x direction at 120 m, 200 m and 280 m.
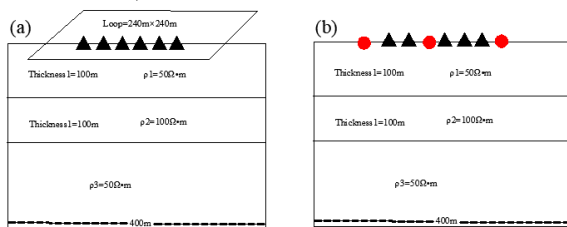

Fig. 4. Schematic of Model 1: (a) model with TEM loop source; (b) model with virtual wave point source.

Fig. 5(a) shows the virtual wave inverted by TSVD. As described in the introduction section, the TEM response is completely within the secondary field, thus the inverted virtual wave response does not include the direct wave.

Receivers were evenly distributed from 140 m to 260 m along the surface. Three different transmitter positions are respectively employed at 120 m, 200 m and 280 m. Fig. 5(a) shows the time profile of inversed virtual wave, which exhibits obvious layered characteristics. Fig. 5(b) shows the apparent

resistivity calculated from the synthetic TEM data. As anticipated, the depth resolution is poor.

Figs. 6(a)–(d) show the results obtained if only data from a single transmitter are virtual-wave transformed and inverted (positions 120 m, 200 m and 280 m, respectively). Each of these inversions yields improved images of the electric model when compared to the apparent resistivity shown in Fig. 5(b). In addition, Fig. 5(f) shows the joint inversion of the data from all three transmitter positions. Compared with the results in Figs. 5(c)–(f), the high layer in Fig. 4(d) is closer to the true model. However, the inversion result below 200 m is not acceptably good, which shows that the method is not sufficient to invert the deep structure of the model.
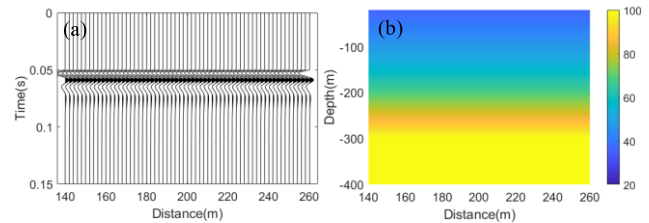

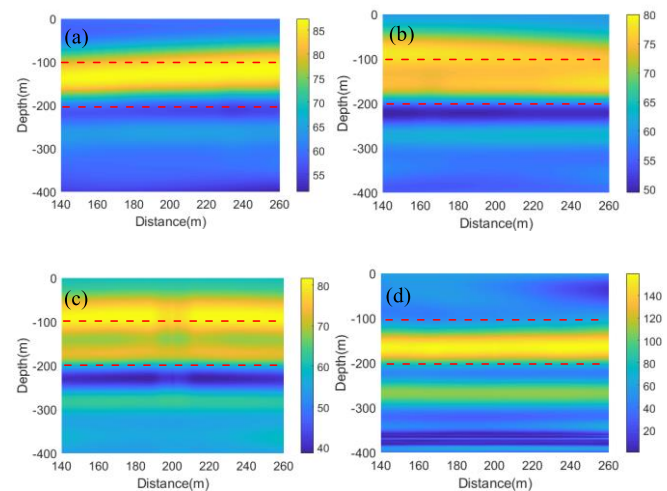Fig. 5. Model 1: (a) inverse virtual wave; (b) apparent resistivity.

Fig. 6. Model 1: (a) inversed virtual wave; (b) apparent resistivity; (c)–(e) FWI based on data from a single transmitter respectively located at 120 m, 200 m and 280 m; (f) FWI based on data from five transmitter positions.

In Model 2, we consider a more complex model, as shown in Fig. 7. It consists of a square of low resistivity body (50×100 m) under a high resistance layer. Figs. 8(a) and (b) respectively show the layouts of the TEM and virtual wave. We see once again that the apparent resistivity computed from the synthetic TEM data is poor in terms of both parameter values and depth resolution, as shown in Fig. 9(b). The results obtained by employing the proposed approach of virtual wave conversion and FWI are shown in Figs. 9(c)–(f).

As observed previously, the use of data from all of source position yields a superior result (Fig. 9(f)) when compared to the use of data from single transmitter positions (Fig. 9(c)–(e)). Moreover, a lower layer is shown at the depth of 200~250 m.
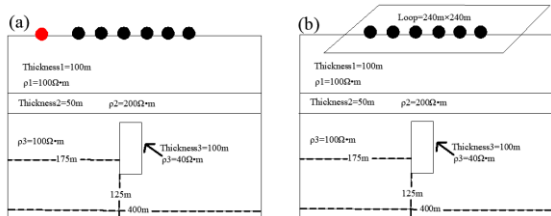
Fig. 7. Schematic of Model 1: (a) model with TEM loop source; (b) model with virtual wave point source.
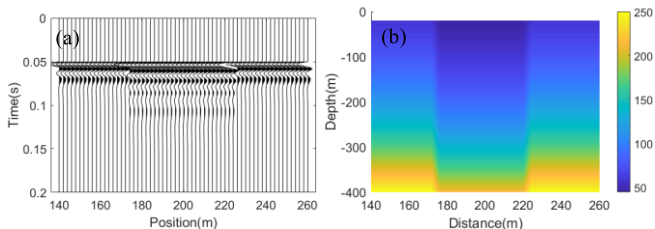

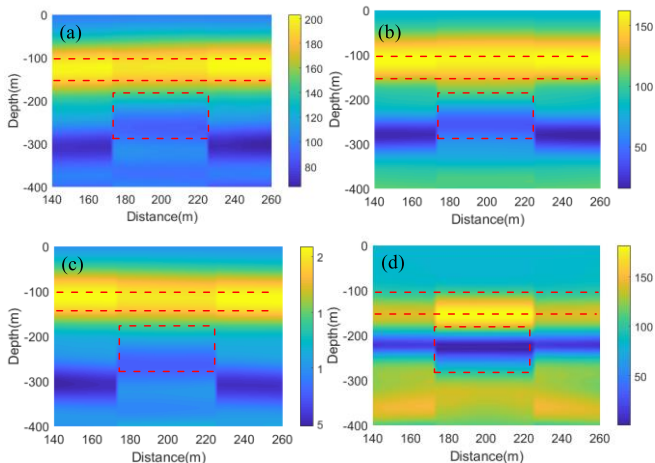Fig. 8. Model 2: (a) inverse virtual wave; (b) apparent resistivity.

Fig. 9. Full waveform inversion results for Model 3: (a)–(c) using data from single transmitters respectively located at 120 m, 200 m and 280 m (marked with a red star); (d) joint inversion employing data from all five transmitters.

VI. FIELD DATA RESULT

In this paper, we present a field data example to illustrate the effectiveness of the proposed method. The TEM field data were acquired at the site of the Halagou Coal Mine in Shenmu County, Shanxi Province, China. Fig. 10(a) shows schematic of the survey area. We choose survey line 5 to apply in this study, a 240×240 m loop-antenna is used as the transmitter, and 22 receiver points are evenly distributed along survey line 5. Fig. 10(b) shows the geological information of drilling HT2 (point 4 in line 8). In addition, a ground magnetic resonance (GMR) measurement is carried out at the location marked HC1 in Fig. 10(a).
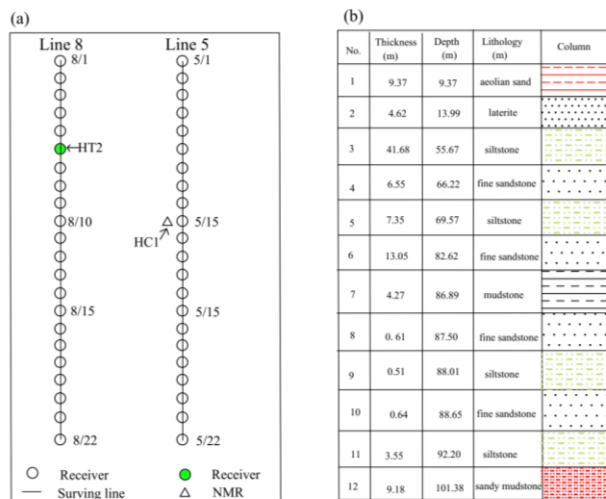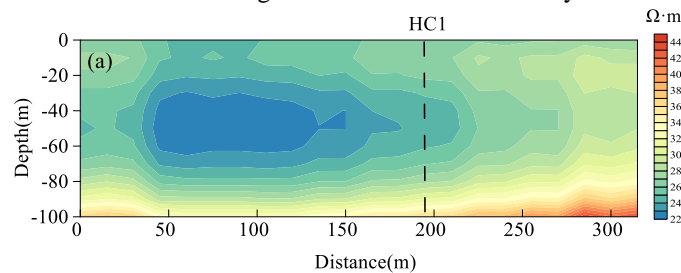

Fig. 10. Schematics of survey area: (a) survey lines; (b) geological information of drilling HT2

According to the relevant information, the survey area shown in Fig. 10(a) is flat, thus the drilling HT2 (Fig. 10(b)) is a very important reference. As shown in Fig. 10(b), the shallow layer of is mainly dominated by the Quaternary system (0–20 m) with corresponding relatively high resistivity. For the deeper parts, it is mainly composed of sandstone and mudstone.

Fig. 11(a) shows the apparent resistivity map calculated from the TEM field data by the Occam inversion method [31]. At the location of the GMR measurements (marked HC1) the apparent resistivity is quite low, except at great depths. If we compare this with the GMR measurements shown in Fig. 11(c), then we can see that the apparent resistivity map may contain well resolved information regarding the aquifer at a depth of about 40 m. However, it has no correlation with the high water content measured at a depth of about 90 m. This is also confirmed by the drilling of borehole HT4.

Fig. 11(b) shows the result obtained employing our proposed approach of FWI processing strategy. If we consider this inversion result at the location of the GMR measurements, then an improved correlation can be seen with these latter measurements in comparison with the apparent resistivity case. The resistivity is relatively low at the depths of 40 m and 85 m, which can match the high water content measured by GMR.
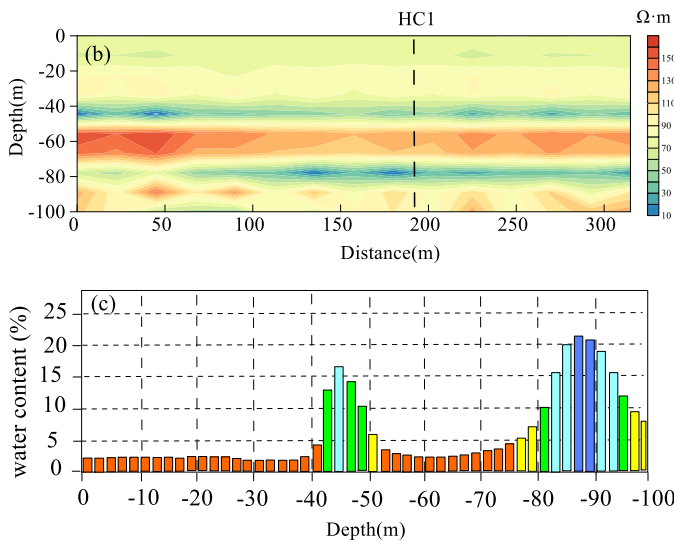
Fig. 11. Schematics of survey area: (a) apparent resistivity result; (b) FWI result; (c) GMR result of HC1.

VII. Conclusion

In the conventional processing of TEM data, the apparent resistivity map plays a key role. However, such plots exhibit poor depth resolution, and yield distorted property values. This observation has motivated the new processing scheme proposed in this paper. As a starting point, we employ the Lee transform (Lee, 1987), then transform the TEM measurements to their pseudo-seismic wave field (or virtual wave field) equivalence. In this way, higher-resolution data can be obtained. Previous work regarding TEM and virtual field transformation has mostly focused on the imaging aspect by means of migration techniques. As an alternative approach, in this paper we propose using the virtual wave field data as the input to FWI. In this manner, both improved depth resolution and accurate parameter estimations can be obtained. Such quantitative results are not achievable with the use of migration techniques, since they only yield structural information. Both simulation and field data are employed to demonstrate the superiority of the proposed methodology when compared with conventional apparent resistivity mapping.

References

[1] W.B. Guo, G.Q. Xue, X. Li, "Correlation analysis and imaging technique of TEM data," *Exploration Geophysics*, vol. 43, no. 3, pp. 137-148, Sep. 2012.

[2] Z. H. Jiang, J. H. Yue, S.C. Liu, "Prediction Technology of Buried Water-Bearing Structures in Coal Mines Using Transient Electromagnetic Method," *Journal of China University of Mining &Technology,* vol. 17, no. 2, pp. 164-167, 2007.

[3] Q.Y. Di, H. Li, G. Q. Xue, L. B. Zhang, "Pseudo-2-D transdimensional Bayesian inversion of the full waveform TEM response from PRBS source," *IEEE Transactions on Geoscience and Remote Sensing*, vol. 58, no. 11, pp. 7602-7610, 2020.

[4] J.L. Cheng, H. Qiu, Y. T. Xie, G.C. Yan, J. Zhou, F.B. Cheng, S.S. Zhang, "Research on wave-field transformation and data processing of the mine transient electromagnetic method," *Journal of China coal society,* vol. 38, no. 9, pp. 1646-1650, Oct. 2013.

[5] B.R. Spies, A.P. Raich, "Calcualtion of Apparent Conductivity for the transient electromagnetic Method," *Geophysics,* vol. 45, no. 7, pp. 1191-1204, Jul. 1988.

[6] A.T. de Hoop, "Transient electromagnetic vs. seismic prospecting—a correspondence principle 1," *Geophysical prospecting,* vol. 44, no. 6, pp. 987-995, Nov. 1996.

[7] F. Collino, C. Tsogka, "Application of the Perfectly Matched Absorbing Layer Model to the Linear Elastodynamic Problem in Anisotropic Heterogeneous Media," *Geophysics*, vol. 66, no. 1, pp. 294-307, Jan. 2001.

[8] P.C.H. Veeken, M. D. Silva, "Seismic Inversion Methods and some of their constraints," *First Break,* vol. 22, no. 6, Jun 2004.

[9] Z.Q. Wu, S.X. Wang, S.H. Zhang, "Application of amplitude ratio profiles extracted with prestack Kirchhoff integral migration," *Petroleum Science,* vol. 4, no. 1, pp. 36-40,Mar. 2007.

[10] G.Q. Xue, Y. J. Yan, X. Li, "Control of Waveform Dispersion Effect and Applications in TEM Imaging Technique for Identifying Underground Objects," *Journal of geophysics and engineering,* vol. 8, no. 2, pp. 195-201, Mar. 2011.

[11] G.Q. Xue, C.Y. Bai, X. Li, "Extracting Virtual Reflection Wave From TEM data Based on Regularizing Method," *Pure and applied geophysics*, vol. 69, no. 7, pp. 1269-1282, Jul. 2012.

[12] K.H. Lee, G.Liu, H.F. Morrison, "A new approach to modeling the electromagnetic response of conductive media", *Geophysics,* vol. 54, no. 9, pp. 1180-1192, Sep. 1989.

[13] R. Mittet, "High-order finite-difference simulations of marine CSEM surveys using a correspondence principle for wave and diffusion fields," *Geophysics,* vol. 75, no. 1, pp. F33-50, Jan. 2010.

[14] G.Q. Xue, Y.J. Yan, X. Li, "Pseudo-seismic wavelet transformation of transient electromagnetic response in engineering geology exploration," *Geophysical Research Letters*, vol. 34, no. 16, pp. 337-396, Aug. 2007.

[15] X. Li, G.Q. Li, Y.N. Liu, "A research on TEM imaging method based on synthetic-aperture technology," *Chinese Journal of Geophysics (in Chinese),* vol. 55, no. 1, pp. 333-340, 2012.

[16] G.Q. Xue, L. J. Gelius, L. Xiu, "3D pseudo-seismic imaging of transient electromagnetic data - a feasibility study," *Geophysical Prospecting*, vol. 61, pp. 561-571, Jun. 2013.

[17] M.Y. Khan, G.Q. Xue, W.Y. Chen, "Analysis of Long-offset Transient Electromagnetic (LOTEM) Data in Time, Frequency, and Pseudo-seismic Domain," *Journal of Environmental & Engineering Geophysics,* vol. 23, no. 1, pp. 15-32, Mar. 2018.

[18] T. Fan, "Method and application on 2D pseudo-seismic inversion of Road-Borehole transient electromagnetic detection in coal mine," *Journal of China Coal Society (in Chinese)*, vol. 44, no. 6, pp. 1804-1816, Jan. 2019.

[19] S. Busch, V. Jan , and H. Vereecken, "Improved Characterization of Fine-Texture Soils Using On-Ground GPR Full-Waveform Inversion," *IEEE Transactions on Geoscience & Remote Sensing*, vol. 52, no. 1, pp. 947-3958. 2014.

[20] A.D. Coster, V. Audrey, C. Gregoire, "Evaluation of pavement layer thicknesses using GPR: A comparison between full-wave inversion and the straight-ray method," *Construction & Building Materials*, vol. 168, pp. 91-104. 2018.

[21] A. Tognarelli, E. Stucchi, A. Mazzotti, "Velocity model estimation by means of Full Waveform Inversion of transmitted waves: An example from a seismic profile in the geothermal areas of Southern Tuscany, Italy," *Geothermics*, vol. 88, no. 6, pp. 101894. 2020.

[22] R. Chen, K.T. Tran, "2D Gauss-Newton full waveform inversion of SH- and Love-waves in the time domain," *Journal of Applied Geophysics,* vol. 191, pp. 104363. Aug. 2021.

[23] A. Tarantolla, "strategy for nonlinear elastic inversion of seismic reflection data," *Geophysics,* vol. 51, no. 10, pp. 1893-1903,Oct. 1986.

[24] C. Lyum, Y. Capdeville, G. Lu, L. Zhao, "Removing the CFL stability criterion of the explicit time-domain very high degree spectral-element method with eigenvalue perturbation," *Geophysics*, vol. 86, pp.1-29, Jun. 2021

[25] M.L. Oristaglio, G.W. Hohmann, "Diffusion of electromagnetic fields into a two-dimensional earth: A finite-difference approach," *Geophysics*, vol. 49, no. 7, pp. 1133-1138, Jun. 1984.

[26] Wang X, Liu S. Noise suppressing and direct wave arrivals removal in GPR data based on Shearlet transform. Signal Processing. 2017 Mar 1;132:227-42.

[27] D. Komatitsch, J. Tromp. "A Perfectly Matched Layer absorbing boundary condition for the second-order seismic wave equation," Geophysical Journal of the Royal Astronomical Society, vol. 154, no. 1, pp. 146-153

[28] Guo K, Labate D, Lim WQ, Weiss G, Wilson E. Wavelets with composite dilations and their MRA properties. Applied and Computational Harmonic Analysis. 2006 Mar 1;20(2):202-36.

[29] J.J.Xue, H.S. Zhong, H.Li, "An improvement to the transformation algorithm for the transmission electromagnet field," *Chinese Journal of Geophysics (in Chinese),* vol. 61, no. 12, pp. 5077-5083, 2018

[30] D.Q. Zhou, L. Tan, H.D. Tan, "Inversion of frequency domain helicopter-borne electromagnetic data with Marquardt's method," *Chinese Journal of Geophysics (in Chinese),* vol. 53, no. 2, pp. 421-427, Jan. 2010.

[31] Hai, L, G. Q. Xue, N. N. Zhou, H. S. Zhong, "Inversion of arbitrary segmented loop source TEM data over a layered earth," *Journal of Applied Geophysics*, vol. 128, pp. 87-95, 206.

Leiv-J. Gelius received a MSc in biophysics in 1980 from the Norwegian Institute of Technology (NTNU, Trondheim, Norway) and a Dr.techn. (PhD) in applied physics in 1993 from the same institution. He worked with the oil company Norsk Hydro from 1981 to 1985 at their R&D centre in Bergen, Norway. From 1985 to 1987 he was a research manager of the Applied Mathematics Group, Centre of Industrial Research (SI), Oslo, Norway. In 1987 he was one of the founders of the consulting company Norwave Development where he served as a Managing Director from 1995 to 1997. Since 1997 he has been a professor at the Department of geosciences, University of Oslo. His main research interests are advanced seismic and radar imaging with applications within geotechnical planning, environmental geophysics, medical diagnostics, non-destructive testing and oil prospecting. Gelius has published more than 120 papers in international journals and conference proceedings with referee.

Xin Wu obtained his Doctorate degree (2018) in Geophysics from the University of Chinese Academy of Sciences. Currently, he is a vice professor in the Key Lab of Mineral Resources of the Chinese Academy of Sciences, with an emphasis in theory, technology and application of the transient electromagnetic method.

Zhao Yang obtained his Bachelor degree (2019) in Geophysics from the JiLin University, he is a Phd student in the Key Lab of Mineral Resources of the Chinese Academy of Sciences, with an emphasis in theory, technology and application of the transient electromagnetic method.

JunJie Xue received the mater degree in applied mathematics from Liaoning University of Technology, Jinzhou, China, in 2019. He is currently study in China University of Mining & Technology, Beijing, for the doctor degree. His research interest includes electromagnetic inversion.

Jiulong Cheng is working in China University of Mining & Technology, Beijing, as a professor. He has been engaging in the research of geophysical prospecting technology in coal mines. His main research direction is the application of seismic prospecting, and electromagnetic prospecting in the fields of mining and **engineering**